Chapter 8
Current Spin-Orbit-Induced Microwave Magnetic Dynamics in Layered Nanostructures

A. M. Korostil and M. M. Krupa

8.1 Introduction

There is much current interest in dynamical processes in magnetically ordered systems both from scientific and technological viewpoints. The special interest is related to the problem of the intercoupling between a spin-polarized electron current and the magnetic dynamics in multilayer magnetic nanostructures that can be exhibited in such phenomena, as magnetic switching and a sustained precession of magnetic order vectors.

The interrelation between the spin-polarized current and magnetic order vectors in magnetic multilayer nanostructures [1–3], permitting their mutual control [4], constitutes the basis of the operation of novel nano-devices [5], some of them with properties of a magnetic random-access memory (MRAM) [6], magnetic logic, and coherent microwave radiation sources that present considerable fundamental and application interest [7, 8]. The operation of these devices can be based on both the spin-polarized current-induced and the current spin-orbit-induced magnetic dynamics including magnetic switching and precession [9–11]. Such phenomena have real potential for application in systems of high-speed magnetic processing information and high-frequency fine-tuned GHz and THz electromagnetic radiation.

The intercoupling between a spin current and magnetic state in magnetic nanostructures constitutes the basis of the current-induced manipulation by magnetic dynamics and vice versa, i.e., the magnetic state-induced manipulation by the spin current [12–15]. The spin current can be converted from an incoming

A.M. Korostil (✉) • M.M. Krupa
Department of Physics of Magnetic Materials and Nanocrystalline Structures, Institute of Magnetism, National Academy of Sciences and Ministry of Education of Ukraine, Prospect Vernadsky, 36-b, Kyiv, 03142, Ukraine
e-mail: amand@rambler.ru

O. Fesenko, L. Yatsenko (eds.), *Nanophysics, Nanomaterials, Interface Studies, and Applications*, Springer Proceedings in Physics 195,
DOI 10.1007/978-3-319-56422-7_8

charge current under internal effective magnetic fields of interactions of a different origin (including *s-d* exchange and spin-orbit interactions) with corresponding features of the action of a spin torque on the magnetic states and their dynamics. Inducing magnetic dynamics such as the spin torque can cause switching and precession of the magnetic order vectors (including ferro- and antiferromagnetic orders) in magnetic nanolayers with ferromagnetic (FM) and antiferromagnetic (AF) interactions. The frequency of the magnetic dynamics is determined by the magnitude of magnetic exchange interaction, which is the largest for antiferromagnetic materials. The prospect of obtaining the technological magnetic nanostructures with low-threshold incoming currents, low power consumption, and controlled high-frequency operation is related to utilization of the spin-orbit effects of the spin polarization and magnetic nanostructures with AF exchange interactions.

Generally, the spin-orbit interaction includes the bulk spin Hall effect (SHE) [12, 13] of the transverse (relatively to an incoming current) deflection of electrons with opposite spins in opposite sides and the inverse spin Hall effect (ISHE) of conversion of a charge current into the transverse spin current. In two-dimensional structures (instance, interfaces), the spin-orbit interaction can be manifested via the Rashba spin-orbit effect [14, 15] of the spin splitting of an electron disperse along an electron wave vector. The impact of the spin current on the magnetic states realizes via the spin torque $\boldsymbol{T}$ [16–18] consisting of so-called field-like and dumping-like parts $\boldsymbol{T}_{||}$ and $\boldsymbol{T}_{\perp}$, respectively, which are related to the effects of magnetic order switching and precession dumping or antidumping. The field-like torque $\boldsymbol{T}_{||}$ originates predominantly by the spin-orbit coupling at the interface in combination with the perturbation of the electron distribution function. The torque $\boldsymbol{T}_{\perp}$ originates predominantly by the perturbation of electronic states by the applied electric field.

The current spin-orbit-controlled microwave magnetic dynamics is realized for nanostructures composed of a heavy metal nanolayer (for instance, Pt, Ta) possessing the strong enough spin-orbit interaction and the adjacent active magnetic nanolayer with a strong exchange interaction attaining maximum values of the order of tens THz in the AF cases. For multisublattice magnetic structures (for instance, for AF), a general magnetic dynamics is a combined effect of dynamics of each of the magnetic sublattices coupled by the strong exchange interaction.

The interconnection between the incoming charge current and magnetic dynamics occurs in the mentioned case via the spin current and the spin transfer effect for each sublattice. In such magnetic systems, the simultaneous action of SHE and the inverse SHE (of the transverse to spin current charge current) results in the feedback between the incoming charge current and the magnetic dynamics. This provides sustained steady-state spin torque magnetic oscillations, convertible via a magnetoresistance effect into an AC voltage and the current-driven high-frequency radiation.

The paper is organized as follows. In Sect. 8.2, features of the scattering of spin currents at the interfaces are studied in multilayer magnetic nanostructures with heavy metal sublayers. Section 8.3 is devoted to the dynamic feedback between a magnetization and controlling incoming charge current in ferromagnetic-layered nanostructures with heavy metal sublayers. The strong spin-orbit interaction, SHE,

and ISHE can provide the robustness of the magnetization precession converting via magnetoresistance effects into microwave radiation. In Sect. 8.4, features of spin pumping and spin transfer torques as two reciprocal phenomena are considered in AF-based nanostructures. Section 8.5 is devoted to the dynamic feedback between the controlling charge current and the magnetic dynamics in AF-layered magnetic nanostructures with heavy metal sublayers. In Sect. 8.6, spin Hall magnetoresistance effect (SME) of the impact of the magnetization dynamics on the resistance of the incoming charge current is considered in the bilayer AF nanostructures with insulating AF layers and adjusted heavy metal sublayers as the result of simultaneous action of SHE and ISHE.

8.2 Spin and Charge Currents in Magnetic Nanostructures with Normal Heavy Metal Sublayers

Features of the electron transport in the mentioned magnetic nanostructures are related to the spin-dependent scattering on interfaces. The electron scattering on the normal metal (NM)/magnetic metal (M) interface represents the special interest for magnetic heterostructures with the strong spin-orbital interaction and SHE. In the ferromagnetic case, by scattering theory [19], the spin current $\boldsymbol{j}_s^{(\mathrm{N|F})}$ through an N|F interface (on the N side, flowing into F) can be expressed in terms of the F magnetization $\boldsymbol{M}$ and the (vector) spin accumulation $\boldsymbol{\mu}_{sN}$ in N:

$$\boldsymbol{j}_{sN}(\boldsymbol{m}) = \left(j_{\uparrow} - j_{\downarrow}\right)\boldsymbol{m}\text{-}\frac{1}{e}\left(G_r\boldsymbol{m}\times(\boldsymbol{m}\times\boldsymbol{\mu}_{sN}) + G_i(\boldsymbol{m}\times\boldsymbol{\mu}_{sN})\right) \tag{8.1}$$

where $\boldsymbol{m} = \boldsymbol{M}/|\boldsymbol{M}|$, $e = -|e|$ is the electron charge, and

$$j_{\uparrow(\downarrow)} = \frac{G_{\uparrow(\downarrow)}}{e}\left[(\mu_{cN} - \mu_{cF}) \pm (\boldsymbol{m}\cdot\boldsymbol{\mu}_{sN} - \mu_{sF})\right] \tag{8.2}$$

is the flow of electrons with spin-up and spin-down along $\boldsymbol{m}$ driven by the difference between effective charge chemical potentials in N and F ($\mu_{cN} - \mu_{cF}$) and the difference between spin accumulations at both sides of the interface ($\boldsymbol{m}\cdot\boldsymbol{\mu}_{sN} - \mu_{sF}$).

The spin-dependent conductance at the interface

$$G_{\uparrow(\downarrow)} = G_0\sum_{nm}\left[\delta_{nm} - |r_{nm}^{\uparrow(\downarrow)}|^2\right] \tag{8.3}$$

where $G_0 = e^2/\hbar$ is the conductance quantum, related to the spin-dependent reflection coefficient $r_{nm}^{\uparrow(\downarrow)}$ corresponding to the electron transition between quantum states n and m in with spin projections $\uparrow$ and $\downarrow$, respectively, in N. Conductance G_r and G_i in (8.1) are determined as real and imaginary parts of the spin-mixing conductance

$$G_{\uparrow\downarrow} = G_0 \sum_{nm} \left[\delta_{nm} - \left(r_{nm}^{\uparrow} \right) \left(r_{nm}^{\downarrow} \right)^* \right] \tag{8.4}$$

i.e., $G_{r(i)} = \mathrm{Re(Im)} G_{\uparrow\downarrow}$ is related to spin-flip electron scattering at the interface.

Due to (8.1), the longitudinal (with respect to the magnetization in F) component of the spin current $(j_\uparrow - j_\downarrow)\boldsymbol{m}$ can flow in a metallic F. At the same time, its transverse components are absorbed at the interface on the atomic length scale and act as a torque on the magnetization. The corresponding spin transfer torque (STT) at the interface is described by the expression

$$\boldsymbol{T}_{\mathrm{STT}} = \frac{\hbar}{2e} \boldsymbol{m} \times \left(\boldsymbol{m} \times \boldsymbol{j}_s^{(N|F)} \right) \tag{8.5}$$

Specially, large STT is realized in the current-in-plane (CIP) configuration with the spin current generated by the SHE [20–22] in the N layer and converted to a magnetization torque by the exchange interaction at the interface. This contributes a so-called "damping-like" torque proportional to G_r with symmetry identical to the exchange-mediated term. On the other hand, the Rashba spin-orbit effect at the interface may generate a spin accumulation that acts on the magnetization exerting a "field-like" torque corresponding to G_i.

8.3 Robustness of Ferromagnetic Dynamics

In ferromagnetic/normal metal heterostructures, the spin pumping and the spin transfer torque are two reciprocal processes that occur concomitantly. Their interplay introduces a dynamic feedback effect interconnecting energy dissipation channels of both magnetization and current. The solution of the spin diffusion process in the presence of the SHE in the NM shows that the dynamic feedback gives rise to a nonlinear magnetic damping that is crucial to sustain uniform steady-state oscillations of a spin Hall oscillator [23–25].

In ferromagnetic (FM)/normal metal (NM) heterostructures, nonlocal effects arise because conduction electrons and magnetization reside in different materials and couple only at the interface. In this regime, spin pumping plays the role of spin electromotive force, which refers to the generation of spin current from a precession FM into the NM [25]. The pumped spin current is accompanied by a backflow of spin current [24, 25], which reacts on the FM through the spin transfer torque (STT). The combined effect of spin pumping and backflow-induced STT renormalizes the spin-mixing conductance at the interface [17, 23]. However, in the presence of the SHE, spin pumping and spin backflow are also connected by the combined effect of the SHE and its inverse process ISHE, which forms a feedback loop as illustrated in Fig. 8.1.

This additional feedback mechanism, proportional to the SH angle squared, θ_s^2, is essential to the electron transport in FM/NM heterostructures. Consequently, this

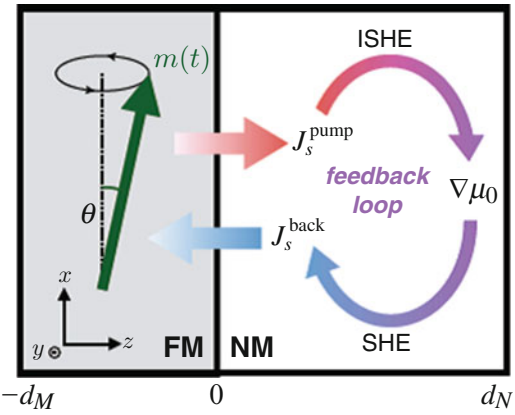

Fig. 8.1 A FM/NMS bilayer, spin pumping, and backflow are connected by the SHE and its inverse process (ISHE)

feedback effect is important to the magnetization dynamics. In a reciprocal sense, if we apply an AC current density to the NM, the SHE will drive the magnetization precession via the STT, which in turn can pump spin current back into the NM and renormalize the resistivity by means of the ISHE.

The feedback effect qualitatively modifies the dynamical behavior of an FM/NM heterostructure. The feedback manifests as a novel nonlinear damping effect in the magnetization dynamics. It enables uniform auto-oscillations of a spin Hall oscillator and prevents magnetic switching. The feedback effect gives rise to a spin Hall magnetoimpedance in the electron transport, which reduces to the observed SMR in the DC limit.

Consider a FM/NM bilayer structure represented in Fig. 8.1 with the layer thicknesses are d_M and d_N, respectively. The coordinate system is chosen such that the magnetization direction at rest is along $\boldsymbol{x}$, and the interface normal is along $\boldsymbol{z}$. It is assumed that the FM is insulating (e.g., YIG), but the essential physics remains valid for a conducting FM since the feedback process takes place only on the NM side. In terms of the electrochemical potential $\mu_0/2$ and the vector of spin accumulation $\boldsymbol{\mu}$ in the NM, the charge and spin current densities J_i^c and $J_{(ij)}^s$, respectively, are described by the expression $J_{i(ij)}^{c(s)} = -\frac{\sigma}{2e}(\partial_i \mu_{0(j)} \pm \theta_s \varepsilon_{ijk} \partial_{j(k)} \mu_k(0))$ with the transport direction i, the spin polarization direction j, the conductivity σ, and the electron charge e. In a given device geometry, only the spin current flowing along z-direction is relevant, and so $\boldsymbol{\mu} = \boldsymbol{\mu}(z, t)$. Correspondingly, the spin (charge) current density reduces to a vector $\boldsymbol{J}_{z(c)}$. The electron and spin dynamics in the NM are described by equations

$$\frac{\partial \boldsymbol{\mu}}{\partial t} = D\frac{\partial^2 \boldsymbol{\mu}}{\partial z^2} - \frac{1}{\tau_{sf}}\boldsymbol{\mu} \tag{8.6}$$

$$\boldsymbol{J}_c = -\frac{\sigma}{2e}\left[\nabla\mu_0 + \theta_s \boldsymbol{z} \times \frac{\partial \boldsymbol{\mu}}{\partial z}\right] \tag{8.7}$$

$$\boldsymbol{J}_{\mathrm{s}} = -\frac{\sigma}{2e}\left[\frac{\partial \boldsymbol{\mu}}{\partial z} + \theta_s \boldsymbol{z} \times \nabla \mu_0\right] \tag{8.8}$$

where D is the diffusion constant and τ_{sf} is the spin-flip relaxation time.

To solve the spin accumulation $\boldsymbol{\mu}$, we assume that the charge current density $\boldsymbol{J}_c$ is fixed by external circuit and is uniform in space. Besides that, we have two boundary conditions $\boldsymbol{J}_s(d_N) = 0$ and

$$\boldsymbol{J}_{s0} = \frac{G_r}{e}\left[\boldsymbol{m} \times (\boldsymbol{m} \times \boldsymbol{\mu}_{s0}) + \hbar \boldsymbol{m} \times \dot{\boldsymbol{m}}\right] \tag{8.9}$$

where $\boldsymbol{\mu}_{s0} = \boldsymbol{\mu}(0)$ and G_r is the real part of the areal density of the spin-mixing conductance and the imaginary part is the real part of the areal density of the spin-mixing conductance (the imaginary part G_i is neglected since $G_r \gg G_i$). In the right-hand side of (8.9), the first term is the STT and the second term is the spin pumping. They are two fundamental ingredients bridging the electron (spin) transport in the NM with the magnetization dynamics of the FM. Due to the conservation of spin angular momentum, the spin current density $\boldsymbol{J}_{s0}$ is absorbed by the FM, which is reflected by the Landau-Lifshitz-Gilbert (LLG) equation

$$\frac{d\boldsymbol{m}}{dt} = \gamma \boldsymbol{H}_{eff} \times \boldsymbol{m} + \alpha_0 \boldsymbol{m} \times \frac{d\boldsymbol{m}}{dt} + \frac{\hbar \gamma_{ex}}{2eM_s d_M} \boldsymbol{J}_{s0} \tag{8.10}$$

M_s is the saturation magnetization, α_0 is the Gilbert damping constant, and $\boldsymbol{H}_{eff}$ is the effective magnetic field.

For typical FMs, the magnetization dynamics is much slower than the spin relaxation rate in the NM so that $\omega r_{sf} \ll 1$. In this limit, the spin accumulation $\boldsymbol{\mu}(z,t)$ adapts to the instantaneous magnetization orientation and is kept quasi-equilibrium. As a result, the spin dynamics described by (8.6) reduces to a stationary spin diffusion process at any specified time. Retaining to second order in θ_s^2 in (8.6) gives

$$\boldsymbol{\mu}(z) = \frac{2e\lambda}{\sigma}\left\{\theta_s \Lambda_1(z) \boldsymbol{z} \times \boldsymbol{J}_c - \Lambda_2(z)\left[\boldsymbol{J}_{s0} + \theta_s^2 \boldsymbol{z} \times (\boldsymbol{z} \times \boldsymbol{J}_{s0})\right]\right\} \tag{8.11}$$

where $\lambda = \sqrt{D\tau_{sf}}$ is the spin diffusion length, $\Lambda_1(z) = \sinh A(z)/\cosh A(0)$, and $\Lambda_2(z) = \cosh B(z)/\sinh B(0)$ with $A(z) = (2z - d_N)/2\lambda$ and $B(z) = (z - d_N)/\lambda$. Here, the t variable in $\boldsymbol{\mu}(z)$ is suppressed since its time dependence simply originates from $\boldsymbol{J}_c$ and $\boldsymbol{J}_{s0}$. The dynamic feedback mechanisms are realized via an effective magnetization dynamics and an effective electron magneto-transport which are described by the system (8.6, 8.7, 8.8, 8.9, 8.10, and 8.11) after elimination electron degrees of freedom ($\boldsymbol{J}_c$ and $\boldsymbol{J}_{s0}$) and the time derivative of the magnetization, respectively.

The DC charge current ($\boldsymbol{J}_c$) applied to normal metal nanolayer (Fig. 8.1), due to the SHE, induces the total spin current density $\boldsymbol{J}_{s0}$ flowing across the interface. The feedback effect is expressed in the intercoupling between the spin current

density $\boldsymbol{J}_{s0}$ and the magnetization $\boldsymbol{m}(t)$ without any electron degree of freedom, by which the LLG (8.10) will no longer involve any electron degrees of freedom. The combination of (8.9) and (8.11) results in two convoluted relations of $\boldsymbol{J}_{s0}$ and $\boldsymbol{\mu}_{s0}$, from which the solution for $\boldsymbol{J}_{s0}$ as a function of $\boldsymbol{J}_c$, $\boldsymbol{m}(t)$ and its time derivative can be obtained. Substituting this solution into (8.10) yields the effective magnetization dynamics

$$\frac{d\boldsymbol{m}}{dt} = \gamma \boldsymbol{H}_{eff} \times \boldsymbol{m} + \omega_s \boldsymbol{m} \times [(z \times \boldsymbol{j}_c) \times \boldsymbol{m}] + \left(\alpha_0 + \alpha_{sp}\right) \boldsymbol{m} \times \frac{d\boldsymbol{m}}{dt} \tag{8.12}$$

where $\boldsymbol{j}_c$ is the unite vector of $\boldsymbol{J}_c$ and

$$\omega_s = \theta_s J_c \frac{\hbar\gamma}{eM_s d_M} \frac{\lambda G_r \tanh \frac{d_N}{2\lambda}}{\sigma + 2\lambda G_r \coth \frac{d_N}{\lambda}} \tag{8.13}$$

is the strength of the STT (driven by $\boldsymbol{J}_c$) scaled in the frequency dimension. The two damping coefficients are described by the expression

$$a_{sp(fb)} = \frac{\left(\lambda\theta_s^2\beta\right)^{0(1)} \hbar^2\gamma}{2e^2 M_s d_M} \frac{\sigma G_r}{(\sigma + 2\lambda G_r \beta)^{1(2)}} \tag{8.14}$$

where $\beta = \coth(d_N/\lambda)$. Here, α_{sp} describes the conventional enhanced damping from spin pumping with the spin backflow effects taken into account [25]; it is independent of the SHE. By contrast, the a_{fb} term reflects the dynamic feedback realized by virtue of the combined effect of the SHE and its inverse process as schematically shown in Fig. 8.1. By virtue of (8.10), this damping term is nonlinear in $\boldsymbol{m}_\perp$ – the component of $\boldsymbol{M}$ transverse to the effective field $\boldsymbol{H}_{eff}$ – whereas the Gilbert damping term is linear in $\boldsymbol{m}_\perp$.

The feedback-induced nonlinear damping effect can be explained in the following way. If the magnetization precession is getting larger, it will trigger a chain reaction: first, the pumped spin current $\boldsymbol{J}_{s0}$ increases, and then the spin diffusion becomes stronger (i.e., $|\partial_z \boldsymbol{\mu}|$ gets larger). This will necessarily lead to a larger $\nabla\mu_0$ in the NM according to (8). Finally, the change of the emf will feed back into $\boldsymbol{J}_{s0}$ according to (8.9), preventing its further increase. Therefore, the growing magnetization precession is inhibited. The entire process realizes a negative feedback.

8.4 Spin Currents in Antiferromagnetic Nanostructures

The spin pumping and spin transfer torque in antiferromagnetic (AF)-based nanostructures represent the combined effect of their action in each of magnetic sublattices coupled by a strong AF exchange interaction. Magnetization dynamics of these

coupled sublattices leads to an AF order ($\boldsymbol{l}$) dynamics manifesting as precession and switching. Similarly to the magnetization in the ferromagnetic case, the AF order precession generates the spin pumping current, which via the ISHE in adjacent nonmagnetic nanolayers can convert into the transverse charge current. Thereby, in AF nanostructures the influence of the AF dynamics on the charge current occurs in AF nanostructures [26]. The inverse impact of the charge current on the AF precession is realized via the SHE effect of the conversion of the charge current into the transverse spin current, which owing to the exchange interaction exerts the spin transfer torque on the AF order precession.

Characteristic features of the AF dynamics and its interconnection with the spin currents in the form of the precession-induced spin pumping and spin transfer torque are manifested in the AF two-sublattice model with an easy axis directed along the axis z and magnetization unit vectors $\boldsymbol{m}_1$ and $\boldsymbol{m}_2$. These vectors are driven by the exchange interaction, the anisotropy, and a magnetic field in the z direction. In units of frequency, they are represented by ω_E, ω_A, and $\omega_H = \gamma H_0$, respectively. The equations of motion in a free precession approximation are

$$\begin{aligned} \dot{\boldsymbol{m}}_1 &= \boldsymbol{m}_1 \times [\omega_E \boldsymbol{m}_2 - (\omega_E + \omega_H)\, \boldsymbol{z}]\,, \\ \dot{\boldsymbol{m}}_2 &= \boldsymbol{m}_2 \times [\omega_E \boldsymbol{m}_1 - (\omega_E - \omega_H)\, \boldsymbol{z}]\,, \end{aligned} \tag{8.15}$$

where the effective field causing the magnetization precession in a magnetic sublattice contains the contribution from the exchange interaction with an adjacent magnetic sublattice. In linear response, when $\boldsymbol{m}_{1(2)} = \pm \boldsymbol{z} - \boldsymbol{m}_{1(2),\perp} \exp i\omega t$ at $|\boldsymbol{m}_\perp| \ll 1$, the resonance frequencies are then

$$\omega = \omega_H \pm \omega_R = \omega_H \pm \sqrt{\omega_A\,(\omega_A \pm 2\omega_E)} \tag{8.16}$$

where the two corresponding eigenmodes are characterized by different chiralities. In the left-handed (right-handed) mode, both $\boldsymbol{m}_1$ and $\boldsymbol{m}_2$ undergo a circular clockwise (counterclockwise) precession with π phase difference. In the absence of magnetic field, viz., $\omega_H = 0$, the two modes are degenerate.

Since without the AF interaction spin current pumped from each of two magnetic sublattices is proportional to $\boldsymbol{m}_{1(2)} \times \partial_t \boldsymbol{m}_{1(2)}$, the total pumped spin current is roughly proportional to $\boldsymbol{l} \times \partial_t \boldsymbol{l}$, where $\boldsymbol{l} = (\boldsymbol{m}_1 - \boldsymbol{m}_2)/2$ denotes the staggered field. The different cone angles θ_1 and θ_2 of $\boldsymbol{m}_1$ and $\boldsymbol{m}_2$, respectively, result in an induced small magnetization $\boldsymbol{m} = (\boldsymbol{m}_1 + \boldsymbol{m}_2)/2$. These cone angles obey the relation $\theta_2/\theta_1 = \eta$, where $\eta \approx \left(1 + \sqrt{\omega_A/\omega_E}\right)^2$.

The spin currents in AF nanostructure determined by mixed scattering channels associated with different sublattices on a N|AF interface. Typical AF materials are insulators, and incident electrons from the normal metal cannot penetrate far. Only a single atomic layer of AF directly connected to N suffices to describe the dominant contribution to interface scattering. Therefore, the essential physics is captured by modeling the N|AF interface as being semi-infinite in the transport direction and infinite in the transverse direction.

Features of kinetics of the polarized electrons in the considered AF nanostructures are described by their scattering matrix (S) near interfaces. In the nearest-neighbor tight-binding model on a cubic lattice, this matrix in a linear in the small magnetization approximation is described by the general expression

$$S = S_0 + S_\omega \tau_1 \sigma_0 + \Delta S \left[\tau_3 \left(\boldsymbol{l} \cdot \boldsymbol{\sigma}\right) + \tau_0 \left(\boldsymbol{m} \cdot \boldsymbol{\sigma}\right)\right] \tag{8.17}$$

where $\boldsymbol{\tau}_{1,2,3}$ are pseudospin Pauli matrices for sublattice degree of freedom, $\boldsymbol{\sigma}$ are the vector of spin Pauli matrices, and τ_0 and σ_0 are identity matrices. The last two terms of (8.17) with a common coefficient ΔS are spin dependent and represent umklapp and normal scatterings, respectively. Pumping currents are related to the coefficients in (8.17) through the spin-mixing conductance $G_{\uparrow\downarrow} = G_r + iG_i$, where

$$G_j = \left(e^2 A/\hbar\pi^2\right) \iint dk_y dk_z \left(\delta_{j,r} |\Delta S|^2 + \delta_{j,i} \operatorname{Im}\left[S_0^* \Delta S\right]\right), \quad j = (r, i),$$

where A is the interface cross section and k_y and k_z are the transverse momenta.

Although the AF resonance frequency reaches the THz region ($1 \sim 10$ meV), the motion of the staggered field remains adiabatic. The spin eigenstates and the scattering matrix (8.17) adiabatically adapt to the instantaneous configuration of AFs. Regarding the staggered field $\boldsymbol{l}$ and the magnetization $\boldsymbol{m}$ as two independent adiabatic parameters [24, 27, 28], the pumped spin current $\boldsymbol{I}_s$ with the scattering matrix can be obtained in the form

$$\boldsymbol{I}_s = \frac{e}{\hbar}\left[G_r\left(\boldsymbol{l} \times \dot{\boldsymbol{l}} + \boldsymbol{m} \times \dot{\boldsymbol{m}}\right) - G_i \dot{\boldsymbol{m}}\right] \tag{8.18}$$

This expression arises from a coherent sum of two independent spin pumping contributions by $\boldsymbol{m}_1$ and $\boldsymbol{m}_2$. Due to the mixing of scattering channels from different magnetic sublattices, the spin-mixing conductance G_r and G_i are different from those of F. Moreover, AF dynamics is much faster than F that corresponds to a stronger spin pumping.

By taking a time average of (8.18) over one period of oscillation, only the first two terms survive and contribute to the DC component of spin current I_s^{dc}. Despite that $|\boldsymbol{m}| \ll |\boldsymbol{l}|$, the contribution of $\boldsymbol{m} \times \partial_t \boldsymbol{m}$ to I_s^{dc} can be comparable to that of $\boldsymbol{l} \times \partial_t \boldsymbol{l}$. This is because I_s^{dc} is proportional to the precession cone angle θ^2 and the cone angle associated with the staggered field is much smaller than the one associated with the magnetization, $\theta_l \approx 0$ but $\theta_m \approx \pi/2$.

From the sublattice degree of freedom involved in the AF dynamics, it follows a staggered spin pumping. A staggered spin current represents the imbalance between the spin current carried by the two sublattices. It has three components $\boldsymbol{I}_{ss}^{(i)}$ ($i = 1$, 2, 3) associated with three pseudo-spin Pauli matrices, from which after the time average only the component

$$\boldsymbol{I}_{ss}^{(3)} = \frac{\hbar}{e} G_r \left(\boldsymbol{l} \times \dot{\boldsymbol{m}} + \boldsymbol{m} \times \dot{\boldsymbol{l}} \right) - G_i \dot{\boldsymbol{l}} \tag{8.19}$$

survives. Elastic scattering in the normal metal will destroy any staggered spin accumulation, which decays on the time scale of $\hbar/t$. Therefore, the staggered spin current is defined within a distance of the mean free path away from the interface.

The reciprocal effect of spin pumping is STT, which describes the back action that a spin current exerts on the AF. In linear response, an AF is driven by two thermodynamic forces $\boldsymbol{f}_l = -\delta F/\delta \boldsymbol{l}$ and $\boldsymbol{f}_m = -\delta F/\delta \boldsymbol{m}$ (energy dimension), where

$$F = \frac{\hbar}{2} \int dv \left[\frac{\omega_0}{a^2} \boldsymbol{m}^2 + \frac{\omega_l}{a\omega_H} \sum_i (\partial_i \boldsymbol{l})^2 \text{-} \omega_H \boldsymbol{H} \cdot \boldsymbol{m} \right] \tag{8.20}$$

is the free energy. Here $\omega_0 = \omega_A + 2\omega_E$ and ω_l are the homogeneous and inhomogeneous exchange frequencies, respectively. Enforced by $\boldsymbol{m} \cdot \boldsymbol{l} = 0$ and $(\boldsymbol{l})^2 \approx 1$, the symmetry allowed dynamics described by the system [25, 26]

$$\hbar \dot{\boldsymbol{l}} = \left(a^3/v \right) \boldsymbol{f}_m \times \boldsymbol{l} \tag{8.21a}$$

$$\hbar \dot{\boldsymbol{m}} = \left(a^3/v \right) \boldsymbol{f}_l \times \boldsymbol{l} + \boldsymbol{f}_m \times \boldsymbol{m} \tag{8.21b}$$

where v is the system volume. Inserting them into (8.18) gives the response of the spin current to $\boldsymbol{f}_m$ and $\boldsymbol{f}_l$. Invoking the Onsager reciprocity relation, we derive the response of $\boldsymbol{l}$ and $\boldsymbol{m}$ to a given spin voltage $\boldsymbol{V}_s$ in the normal metal, which are identified as two STT terms $\boldsymbol{T}_l$ and $\boldsymbol{T}_m$. To linear order in $\boldsymbol{m}$

$$\begin{aligned} \boldsymbol{T}_l &= -\tfrac{a^3}{ev} \left[G_r \boldsymbol{l} \times (\boldsymbol{m} \times \boldsymbol{V}_s) - G_i \boldsymbol{l} \times \boldsymbol{V}_s \right], \\ \boldsymbol{T}_m &= -\tfrac{a^3}{ev} G_r \boldsymbol{n} \times (\boldsymbol{m} \times \boldsymbol{V}_s), \end{aligned} \tag{8.22}$$

that treats STTs on the two sublattices as completely independent.

In solving the AF dynamics, it is instructive to eliminate magnetization and derive a closed equation of motion in terms of $\boldsymbol{l}$ alone [27–30]. In the linear approximation in $\boldsymbol{V}_s$, $\boldsymbol{m}$, and $\partial_t \boldsymbol{l}$, the effective dynamics is described by the equation

$$\boldsymbol{l} \times \left(\ddot{\boldsymbol{l}} + \alpha \omega_0 \dot{\boldsymbol{l}} + \omega_R^2 \boldsymbol{l}_\perp \right) = \frac{\omega_0 a^3 G_r}{ev} \boldsymbol{l} \times \boldsymbol{l} \times \boldsymbol{V}_s \tag{8.23}$$

where α is the Gilbert damping constant and $\boldsymbol{l}_\perp$ are perpendicular components of $\boldsymbol{l}$ with respect to the easy axis. Since the STT only acts on the interface for a thin AF film, a possible nonuniform motion of $\boldsymbol{l}$ is disregarded.

At small enough $\boldsymbol{V}_s$ collinear with the easy axis, the solution for a spectrum of (8.23) characterizes by a negative imaginary part of the frequency ω so that any perturbed motion will decay exponentially in time and the system is stable. However, a sufficiently large $\boldsymbol{V}_s$ flips the sign of $\mathrm{Im}[\omega]$, which makes the system

unstable and marks the onset of uniform AF excitation. The condition $\mathrm{Im}[\omega] = 0$ determines the threshold spin voltage $V_s^{th} = \pm (ev\ \alpha\ \omega_l) / \left(a^3 G_r\right)$, where $+(-)$ corresponds to the excitation of the right-handed (left-handed) mode.

8.5 Dynamic Feedback in Antiferromagnetic/Spin Hall Structures

In the framework the current-induced dynamics of insulating antiferromagnets in a spin Hall geometry and sufficiently large in-plane currents perpendicular to the Néel AF order can trigger spontaneous oscillations at frequencies between the acoustic and the optical eigenmodes [17, 23, 26]. The direction of the driving current determines the chirality of the excitation. When the current exceeds a threshold, the combined effect of current-induced torques and spin pumping introduces a dynamic feedback that sustains steady-state oscillations with amplitudes controllable via the applied current. This permits to obtain the SH nano-oscillator with operating frequencies in THz range.

When an applied STT compensates the magnetic damping, the magnetization becomes unstable: it either switches to another direction or evolves into a steady-state oscillation. While the former improves writing operations in magnetic memory devices, the latter enables sustainable AC signal generation from DC inputs, giving rise to spin torque oscillators (STOs) [31, 32]. In ferromagnets, currents or magnetic fields can tune the STO output frequency from the MHz to the GHz regime.

STOs can potentially be operated at much higher THz frequencies when antiferromagnets (AFs) replace ferromagnets. It is possibly owing to the THz range of the eigenfrequencies of typical AFs and possibility of spontaneous excitations of an AF by anti-damping STTs. While most AFs are insulators where STTs cannot be operated by passing through a current, the SHE can produce STTs even when electrons do not flow through the magnet [31]. Therefore, integrating STOs with the SHE paves the way toward low-dissipation spin Hall nano-oscillators (SHNOs) [6].

However, to realize AF-based SHNOs, current-induced excitations should not grow indefinitely, but instead should evolve into steady-state oscillations and generate a substantial AC output. Although an AF under the action of an anti-damping STT does not suffer magnetic switching, its Néel AF vector experiences either no dynamics or a right-angle precession around the direction of the spin accumulation [18]. Since the oscillation amplitude is not continuously tunable via the applied current, the device does not meet the requirements of an SHNO.

Steady-state oscillations are realizable in ferromagnetic STOs for the following reasons. In a spin valve device, the angle dependence of the Gilbert damping and that of the anti-damping STT differs. As a result, when the driving current is above the threshold, there exists a unique angle where the two competing effects compensate.

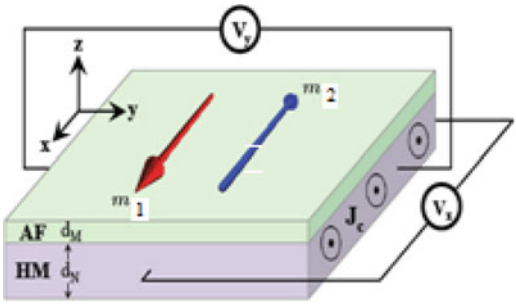

Fig. 8.2 An insulating AF/HM heterostructure. The applied DC current density $\boldsymbol{J}_c$ drives the AF via the SHE. The dynamics of the AF pumps spin current back into N, and converts into electric field via the ISHE, which is monitored by two voltmeters

Then, a steady-state oscillation is stabilized at that angle. However, this features no longer active where the SHE creates the anti-damping STT. Therefore, one needs to introduce alternative mechanisms to prevent a spontaneous excitation from growing into magnetic switching.

Solution of the mentioned problem is based on the use of a feedback mechanism [17] that is realizable in an AF/heavy metal heterostructure. The feedback effect originates from the combined effect of the SHE and its reverse process that connects the spin pumping with the spin backflow [33, 34], which is independent of the dipolar interaction. The threshold of spontaneous excitations is determined via solving the AF order dynamics in the linear response regime. The correlation between the threshold and a current density is related to the SHE in the heavy metal. The feedback is indispensable to sustain uniform auto-oscillation properties of magnetic dynamics of the AF in device geometry in Fig. 8.2 and can be described in the framework of two-sublattice crystal structure with the magnetizations vectors $\boldsymbol{m}_1$ and $\boldsymbol{m}_2$.

The magnetic dynamics is characterized by the AF vector $\boldsymbol{l} = (\boldsymbol{m}_1 - \boldsymbol{m}_2)/\boldsymbol{2}$ and the small magnetization $\boldsymbol{m} = (\boldsymbol{m}_1 + \boldsymbol{m}_2)/\boldsymbol{2}$ and angular frequencies $\omega_\perp$, $\omega_{\shortparallel}$, and ω_E corresponding to the hard axis, easy plane anisotropy, and the Heisenberg exchange interaction, respectively. In the macrospin description, the free energy is

$$F = -\hbar\omega_3 \boldsymbol{l}^2 - \hbar \sum_{i=1,2} \frac{\omega_i}{2} \left((\boldsymbol{r}_i \boldsymbol{l})^2 + (\boldsymbol{r}_i \boldsymbol{m})^2 \right) \tag{8.24}$$

where $\omega_3 = \omega_E + \omega_\perp$, $\omega_{1(2)} = \omega_E + \omega_{\shortparallel(\perp)}$, and $\boldsymbol{r}_{1(2)} = \boldsymbol{x}(z)$, which defines thermodynamic forces, $\hbar \boldsymbol{f}_{l(m)} = -\partial F / \partial \boldsymbol{l}(\boldsymbol{m})$. The coupled equations of motion are

$$\dot{\boldsymbol{l}} = \boldsymbol{f}_2 \cdot (\boldsymbol{m}, \boldsymbol{l}) + \alpha \left(\boldsymbol{m} \times \dot{\boldsymbol{l}} + \boldsymbol{l} \times \dot{\boldsymbol{m}} \right) + \boldsymbol{T}_l \tag{8.25}$$

$$\dot{\boldsymbol{m}} = \boldsymbol{f}_1 \cdot (\boldsymbol{m}, \boldsymbol{l}) + \alpha \left(\boldsymbol{m} \times \dot{\boldsymbol{m}} + \boldsymbol{l} \times \dot{\boldsymbol{l}} \right) + \boldsymbol{T}_m \tag{8.26}$$

where $\boldsymbol{f}_{1(2)} = (\boldsymbol{f}_{m(l)}\times, \boldsymbol{f}_{l(m)}\times)$, (here the sign "×" denotes the vector multiplication), α is the Gilbert damping constant, and the STTs given (see [13, 21]) by

$$\begin{aligned} \boldsymbol{T}_m &= \boldsymbol{l}\times(\boldsymbol{\omega}_s\times\boldsymbol{l}) + \boldsymbol{m}\times(\boldsymbol{\omega}_s\times\boldsymbol{m}), \\ \boldsymbol{T}_l &= \boldsymbol{l}\times(\boldsymbol{\omega}_s\times\boldsymbol{m}) + \boldsymbol{m}\times(\boldsymbol{\omega}_s\times\boldsymbol{l}). \end{aligned} \tag{8.27}$$

Here the STT strength is determined via the vector of spin accumulation $\boldsymbol{\omega}_s$. The vector decomposition $\boldsymbol{l} = \boldsymbol{x} + \boldsymbol{l}_\perp \exp i\omega t$ in (8.26) results in the eigenfrequency expression

$$\omega_\pm = i\omega_E\alpha + \left[\omega_E^2\omega' \pm \omega_E\sqrt{\omega_\perp^2 - 4\omega_s^2}\right]^{1/2} \tag{8.28}$$

where $\omega' = \omega_\perp + 2\omega_{||} - \alpha^2$, + (−) denotes the optical (acoustic) mode. As ω_s increase, the real parts Re[ω_+] and Re[ω_-] approach each other until they become degenerate at $\omega_s = \omega_\perp/2$. The imaginary parts Im[ω_+] and Im[ω_-] remain degenerate and unaffected for $\omega_s < \omega_\perp/2$. When $\omega_s > \omega_\perp/2$, Im[$\omega_+$] (Im[$\omega_-$]) reduces (grows) rapidly, indicating that the damping is diminished (enhanced) by the STT.

At the threshold [18],

$$\omega_s^{th} = \sqrt{\frac{\omega_\perp^2}{4} + \alpha^2\left(2\omega_{||} + \omega_\perp\right)\omega_E} \tag{8.29}$$

Im[ω_+] vanishes, which marks the onset of spontaneous excitation of the optical mode and the breakdown of the linear response approximation. The uniaxial symmetry enforces that Im[ω_+] also vanishes for the threshold so that the auto-oscillation can be triggered by a reversed current as well.

In the absence of the hard axis anisotropy, the threshold (8.29) is linear in α, so the anti-damping effect occurs when the STT is turned on. However, in the general case where $\omega_\perp > 0$, the anti-damping effect appears only when $\omega_s > \omega_\perp/2$. Vectors $\boldsymbol{m}_1$ and $\boldsymbol{m}_2$ always exhibit opposite chiralities, i.e., they rotate counterclockwise (clockwise). However, at the degenerate point $\omega_s = \omega_\perp/2$, the chirality of $\boldsymbol{m}_1(\boldsymbol{m}_2)$ in the optical (acoustic) mode reverses. At $\omega_s > \omega_\perp/2$, both $\boldsymbol{m}_1$ and $\boldsymbol{m}_2$, hence the Néel vector $\boldsymbol{l}$, all acquire the same chirality. At the threshold ω_s^{th}, the excited optical mode is right handed. If ω_s changes sign, the optical mode is still excited, but its chirality becomes left handed. These suggest that the direction of the current determines the chirality of the excitation.

In the considered two-layered nanostructure, insulating AF/heavy normal metal (HM) with strong spin-orbit coupling (Fig. 8.2), a current density $\boldsymbol{J}_c$ is applied along the direction perpendicularly to the AF vector $\boldsymbol{l}$. The SHE in the HM generates anti-damping STTs to drive the AF vector dynamics, which in turn pumps spin current back into the HM. The pumped spin current converts into a charge voltage due to the inverse SHE. The spin diffusion equation in the presence of the SHE under boundary conditions involving both spin pumping and STT results in the expression

$$J_c^{th} = \omega_c^{th} \frac{d_M \left(\hbar\sigma + 2\lambda e^2 G_r \coth \frac{d_N}{\lambda}\right)}{2\theta_s \alpha^3 \lambda e G_r \tanh \frac{d_N}{\lambda}} \tag{8.30}$$

describing the dependence of the a critical current density on the threshold STT (8.29), the spin Hall angle θ_s, and the areal density of transverse mixing conductance G_r^t. From (8.30) it is follows that the critical current density J_c^{th} can be lowered by reducing (increasing) the thickness of the AF d_M (HM d_N).

The sustained steady-state oscillation of the AF vector in the mentioned nanostructure can be realized via the dynamic feedback effect. The pumped spin current from a precessing AF vector into the HM experiences a backflow [33, 34]. In HMs, however, the spin pumping and the spin backflow are also connected via the combined effect of the SHE and its inverse process, which feeds the Néel vector dynamics back into itself. In ferromagnets, such a feedback mechanism manifests as a nonlinear damping effect in the magnetization dynamics. Similar feedback-induced damping effect can occur for AFs. In this case, the pumped spin current into the HM converts into an electric field $\boldsymbol{E}$ due to ISHE. According to Ohm's law,

$$\boldsymbol{J}_c = \sigma \boldsymbol{E} - \theta_s \left(\sigma/2e\right) \boldsymbol{z} \times \partial_z \boldsymbol{\mu}_s \tag{8.31}$$

where $\boldsymbol{\mu}_s$ is the spin accumulation in the HM. At the fixed current density $\boldsymbol{J}_c$ through external circuits, a change of the electric field $\boldsymbol{E}$ necessarily leads to a change of the spin accumulation. Subsequently, the change of $\boldsymbol{\mu}_s$ diffuses and generates an additional spin current, which will finally deliver the influence of spin pumping back into the AF vector through STTs. Closing such a feedback loop results in a feedback torque that should be added to (8.27) as

$$\boldsymbol{T}_{FB} = \alpha_{NL} \left[l_z^2 \boldsymbol{l} \times \dot{\boldsymbol{l}} - \dot{l}_z \left(\boldsymbol{z} \times \boldsymbol{l}\right) \right] \tag{8.32}$$

where the feedback coefficient is

$$a_{NL} = \frac{\theta_s^2 \alpha^3}{d_M} \frac{2\hbar – e^2 G_r^2 \coth \frac{d_N}{\lambda}}{\left(h\sigma + 2\lambda e^2 G_r \coth \frac{d_N}{\lambda}\right)} \tag{8.33}$$

While the feedback effect seems to be a higher-order effect as a_{NL} is proportional to θ_s^2, it can be significantly enhanced by searching for materials with large θ_s. The feedback-induced nonlinear damping is a critical ingredient because it dramatically modifies the dynamical behavior of an SHNO using AF.

A salient feature of the considered stable oscillation phase is that the applied DC current density $\boldsymbol{J_c}$ controls the output power and that the output power is substantial that is indispensable for an SHNO. In the stable oscillation phase, the actual frequency output lies between the acoustic and the optical modes. The AC voltage output is determined by ISHE and the spin pumping. For a fixed $\boldsymbol{J}_c$ the total electric field $\boldsymbol{E} = \boldsymbol{J}_c/\sigma + \Delta \boldsymbol{E}$ includes a time-varying part

$$\Delta \boldsymbol{E} = \frac{\theta_s \hbar}{d_N} \frac{\lambda e G_r \tanh \frac{d_N}{2\lambda}}{h\sigma - 2\lambda e^2 G_r \coth \frac{d_N}{\lambda}} \left(\boldsymbol{l} \times \dot{\boldsymbol{l}} \right) \times \boldsymbol{z} \tag{8.34}$$

A time average of (8.34) results in the effective value of the components $\overline{E}_x$ and $\overline{E}_y$ which are appreciably large in the stable oscillation phase.

8.6 Spin Hall Magnetoresistance in Magnetic Nanostructures

Interconnection between the magnetic dynamics in magnetic layers and the charge current in the adjacent nonmagnetic heavy metal (HM) nanolayers with the strong spin-orbit interaction can exhibit via the so-called spin Hall magnetoresistance effect (SME) [35, 36] of the magnetic-induced change of the charge current. The impact of the magnetic dynamics on the charge current in nonmagnetic layers is related to a nonequilibrium proximity effect caused by the simultaneous action of the SHE and ISHE [37, 38]. The impact of the magnetization on the charge current occurs via the magnetic-induced variation of the nonequilibrium spin diffusion in the normal metal layers at the interface, converting by the ISHE into the charge current. Herewith, the spin diffusion occurs from the dynamic state of the spin accumulation caused by the interface reflection of the SHE-induced spin current. The spin diffusion current is in direct dependence on the exchange interaction between the magnetization and the spin current nearby the interface.

Especially clearly, SME is exhibited in the case of insulating magnetic (IM) nanolayer (specifically, yttrium iron garnet (YIG)) adjusting to the HM nanolayer (specifically, Pt) possessing the strong enough spin-orbit interaction. When a charge current $\boldsymbol{J}_c$ is sent through a Pt nanolayer, a transverse spin current $\boldsymbol{J}_s$ is generated by the SHE following $\boldsymbol{J}_c \propto \sigma \times \boldsymbol{J}_s$, where σ is the polarization direction of the spin current. Part of this spin current is directed toward the interface as is shown in Fig. 8.3.

At the interface, the electrons in the Pt will interact with the localized moments in the YIG. Depending on the magnetization ($\boldsymbol{M}$) direction of the YIG, electron spins will be absorbed ($\boldsymbol{M} \perp \sigma$) or reflected ($\boldsymbol{M} \| \sigma$). By changing the direction of the magnetization of the YIG, the polarization direction of the reflected spins and thus the direction of the additional created charge current can be controlled. A charge current with a component in the direction perpendicular to $\boldsymbol{J}_e$ can also be created, which generates a transverse voltage.

In a diffusion approximation for both magnetic and HM nanolayers, the spin and charge currents are expressed in terms of gradients of charge and spin accumulations (or spin-dependent electrochemical potentials and densities). The charge current density is the expectation value of the current operator $\boldsymbol{j} = e(n\boldsymbol{v} + \boldsymbol{v}n)/2$, where e is the electron charge, n is the electron density, and $\boldsymbol{v}$ is the velocity operator. For a normal metal with constant density n_N and rift velocity $\boldsymbol{v}_N$, $\boldsymbol{j}_{eN} = en_N\boldsymbol{v}_N$. The spin current in the nonrelativistic limit is the second-order tensor

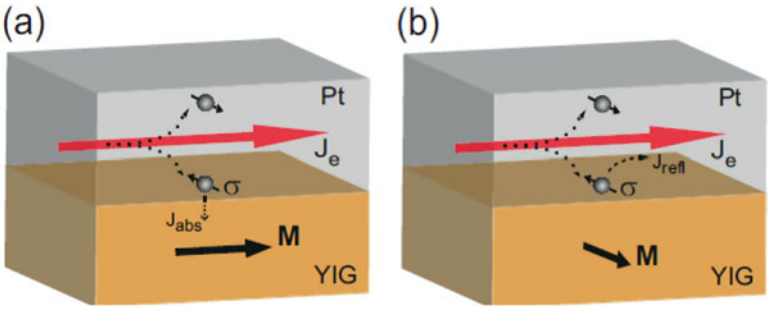

Fig. 8.3 Schematic of the passage of spin and charge currents at the SME in a YIG/Pt nanostructure. (**a**) When the magnetization $\boldsymbol{M}$ YIG is perpendicular to the spin polarization σ of the spin accumulation created in the Pt by the SHE, the spin accumulation will be absorbed ($\boldsymbol{J}_{\text{abs}}$) by the localized moments in the YIG. (**b**) For $\boldsymbol{M}$ parallel to σ, the spin accumulation cannot be absorbed, which results in a reflected spin current back into the Pt, where an additional charge current $\boldsymbol{J}_{\text{refl}}$ will be created by the ISHE

$$\overleftrightarrow{\boldsymbol{j}}_{sN} = \frac{e}{2}\langle \boldsymbol{j} \otimes \sigma + \sigma \otimes \boldsymbol{j} \rangle = \left(\boldsymbol{j}_{sx}, \boldsymbol{j}_{sy}, \boldsymbol{j}_{sz}\right)^T \tag{8.35}$$

where σ is the vector of Pauli spin matrices, $\otimes$ denotes the tensor product, and $<\cdots>$ denotes an expectation value. The row vectors $\boldsymbol{j}_{si} = en(\boldsymbol{v}\sigma_i + \sigma_i \boldsymbol{v})/2$ are the spin current densities polarized in the i-direction. In metallic ferromagnets with homogenous texture, the average spin current is projected along the unit vector of the magnetization direction $\boldsymbol{m}$, so the charge current and spin current tensor have the form

$$\begin{aligned} \boldsymbol{j}_{cF} &= e\left(n_{\uparrow F}\boldsymbol{v}_{\uparrow F} + n_{\downarrow F}\boldsymbol{v}_{\downarrow F}\right), \\ \overleftrightarrow{\boldsymbol{j}}_{sF} &= \boldsymbol{j}_{sF} \otimes \boldsymbol{m} = \left(\boldsymbol{j}_{\uparrow F} \boldsymbol{j}_{\downarrow F}\right) \otimes \boldsymbol{m}, \end{aligned} \tag{8.36}$$

where $\boldsymbol{j}_{cF}$ is the spin current density direction vector.

In the diffusion approach and the two-channel model, currents close to the interface of the heterostructure are determined via gradients of the spin-dependent chemical potentials $\mu_{\varsigma F}$, $\boldsymbol{j}_{\varsigma F} = -(\sigma_{\varsigma F}/e)\nabla\mu_{\varsigma F}$, where $\varsigma = (\uparrow, \downarrow)$ represents the spin direction along of the magnetization and $\sigma_{\varsigma F}$ is the spin-dependent conductivity. The charge current $\boldsymbol{j}_{cF} = \boldsymbol{j}_{\uparrow F} + \boldsymbol{j}_{\downarrow F}$ and the spin current $\boldsymbol{j}_{sF} = \boldsymbol{j}_{\uparrow F} \boldsymbol{j}_{\downarrow F}$ are expressed via charge and spin chemical potentials $\mu_{cF} = (\mu_{\uparrow F} + \mu_{\downarrow F})/2$ and $\mu_{sF} = (\mu_{\uparrow F} - \mu_{\downarrow F})/2$, respectively. These currents are described by the general expression [37]

$$\boldsymbol{j}_i = -\frac{\sigma_F}{e}\left[\delta_{i,cF}\left(\nabla\mu_{cF} + \frac{1}{2}P\nabla\mu_{sF}\right) + \delta_{i,sF}\left(P\nabla\mu_{cF} + \frac{1}{2}\nabla\mu_{sF}\right)\right], \; i = (cF, sF) \tag{8.37}$$

where $P=(\sigma_{\uparrow F}-\sigma_{\downarrow F})/(\sigma_{\uparrow F}+\sigma_{\downarrow F})$. The abovementioned potentials are determined by the diffusion equations

$$\nabla^2\mu_{sF}=\frac{\mu_{sF}}{\lambda_F^2},\quad \nabla^2\left(\mu_{cF}+P\mu_{sF}/2\right)=0 \tag{8.38}$$

where the spin-flip diffusion length $\lambda_F=\left(\lambda_{\uparrow F}^{-2}+\lambda_{\downarrow F}^{-2}\right)^{-1/2}$ is expressed in terms of the spin diffusion lengths $\lambda_{\varsigma F}=\sqrt{D_{\varsigma F}\tau_{sf,\varsigma F}}$ for each spin ($\tau_{\varsigma f,sF}$ is the spin-dependent spin-flip time). The spin-dependent charge diffusion constant $D_{\varsigma F}=\tau_{\varsigma F}v_{\varsigma F}^2/3$ depends on the spin-dependent relaxation time $\tau_{\varsigma F}$ and Fermi velocity v_ς. Solutions of (8.38), corresponding to boundary conditions at interface, due to (8.37) determine the charge and spin currents.

In normal metals, the induced spin accumulations are represented by the (position-dependent) vector $\boldsymbol{\mu}_{sN}=(\mu_{sx},\mu_{sy},\mu_{sz})^T-\mu_{cN}1$, components of which together with the charge chemical potential obey the diffusion equation system

$$\nabla^2\mu_{si}=\frac{\mu_{si}}{\lambda^2},\quad \nabla^2\mu_{cN}=0 \tag{8.39}$$

Without the SHE, charge and spin currents are expressed by the system

$$\boldsymbol{j}_{cN}=-\frac{\sigma_{cN}}{e}\nabla\mu_{cN},\ \boldsymbol{j}_{si}=-\frac{\sigma_{si}}{e}\nabla\mu_{si} \tag{8.40}$$

The spin polarization in the case of the NM layers has arbitrary direction in contrast to the case of the magnetic layers.

In the considered case of the bilayer nanostructure HM/FI (FI denotes insulating magnetic) represented in Fig. 8.4, the charge current flow in the metal parallel to the applied electric field $\boldsymbol{E}$ and the SHE generate a spin accumulation. The generalized Ohm's law in this can be represented by the system [19]

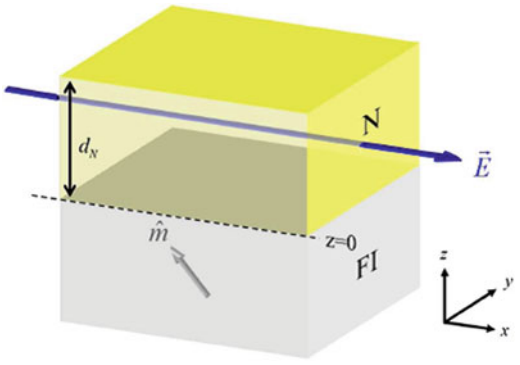

Fig. 8.4 The N|FI bilayer structure with the charge flow along an electric field $\boldsymbol{E}$

$$\boldsymbol{j}_{si} = \frac{\sigma_N}{e}\left(\theta_S \boldsymbol{x}_i \times \nabla\mu_{cN} + \frac{1}{2}\nabla\mu_{sx_i}\right) \tag{8.41}$$

$$\boldsymbol{j}_{cN} = \frac{\sigma_N}{e}\left(\nabla\mu_{cN} + \frac{\theta_S}{2}\sum_i \boldsymbol{x}_i \times \nabla\mu_{sx_i}\right) \tag{8.42}$$

where $\boldsymbol{\mu}_{sN} = (\mu_{sx}, \mu_{sy}, \mu_{sz})^T - \mu_{cN}\mathbf{1}$ is the spin accumulation, i.e., the spin-dependent chemical potential relative to the charge chemical potential $\mu_{cN} = e\varphi$, σ_N is the electric conductivity, and "×" denotes the vector product operating on the gradients of the spin-dependent chemical potentials. The SHE is governed by the first term in (8.41) that generates the spin currents parallel to the applied electric field $\boldsymbol{E} = E_x\boldsymbol{x}$ (Fig. 8.4). The ISHE is governed by the second term in (8.42) that connects the gradients of the spin accumulations to the charge current density.

According to (8.41) and (8.42), the spin current in N consists of conventional diffusion and spin Hall drift contributions. The spin current density flowing in the z-direction is described by the expression

$$\boldsymbol{j}_{sz} = -\frac{\sigma_N}{2e}\nabla_z\boldsymbol{\mu}_{sN} - j_{s0}^{SH}\boldsymbol{y} \tag{8.43}$$

where $j_{s0}^{SH} = \theta_S\sigma_N E_x$ is the bare spin Hall current, i.e., the spin current generated directly by the SHE. Due to the boundary conditions, $\boldsymbol{j}_{sz}(z)$ is continuous at the interfaces $(z = d_N, 0)$. The spin current density at a vacuum interface $(z = d_N)$ vanishes, while at the magnetic interface $(z = 0)$, it is governed by the spin accumulation and spin-mixing conductance according to (8.1), $\boldsymbol{j}_{sz}(0) = -\boldsymbol{j}_s^{(\mathrm{N|F})}$. With these boundary conditions, solution of (8.39) for the spin accumulation is described by the expression

$$\frac{\boldsymbol{\mu}_{sN}(z)}{\mu_s^0} = -\boldsymbol{y}\frac{\sinh A(z)}{\sinh A(0)} - \frac{2\lambda\cosh B(z)}{\sinh B(0)}\left[\boldsymbol{m}\times(\boldsymbol{m}\times\boldsymbol{y})\,\mathrm{Re} + (\boldsymbol{m}\times\boldsymbol{y})\,\mathrm{Im}\right]\varphi\left(G_{\uparrow\downarrow}\right) \tag{8.44}$$

where $A(z)$ and $B(z)$ were defined in (8.11), $\varphi(z) = z(\sigma_N + 2\lambda z\coth B(2d_N)^{-1}$, and μ_s^0 is the spin accumulation at the interface in the absence of spin transfer. By virtue of (8.44), the spin current in N is described by the expression

$$\frac{\boldsymbol{j}_s^z(z)}{j_{s0}^{SH}} = \boldsymbol{y}\left(\Delta_1(z) - 1\right)\text{-}\Delta_2(z)\ \mathbf{R}\ \varphi\left(G_{\uparrow\downarrow}\right) \tag{8.45}$$

where

$$\Delta_1(z) = \frac{\cosh A(z)}{\cosh A(0)},\quad \Delta_2(z) = \frac{2\lambda\tanh A(0)\sinh B(z)}{\sinh B(0)}$$

R denotes the expression emphasized by squared brackets in (8.44). The spin current at the interface N|F vanishes when the magnetization is along $\boldsymbol{y}$. The spin current at the interface and the torque on the magnetization are activated, while the spin accumulation is dissipated by rotation of the magnetization from $\boldsymbol{y}$ to $\boldsymbol{x}$. The $\boldsymbol{x}$-components of both spin accumulation and spin current vanish when the magnetization is along $\boldsymbol{x}$ and $\boldsymbol{y}$ and are largest at $(\boldsymbol{x}+\boldsymbol{y})/2$.

The ISHE drives a change current in the x - y plane by the diffusion spin current component flowing along y-direction. The total longitudinal (along $\boldsymbol{x}$) and transverse (along $\boldsymbol{y}$) charge currents [37]

$$\frac{j_{cx}(z)}{\sigma_N E_x} = 1 + \theta_S^2 \left[\Lambda_1(z) + \left(1 - m_y^2\right) \Lambda_2(z)\, \mathrm{Re}\varphi\left(G_{\uparrow\downarrow}\right)\right] \tag{8.46}$$

$$\frac{j_{cy}(z)}{\sigma_N E_x} = \theta_S^2 \Lambda_2 \left(1 - m_y^2\right) \left[m_x m_y\, \mathrm{Re} - m_z\, \mathrm{Im}\right] \varphi\left(G_{\uparrow\downarrow}\right) \tag{8.47}$$

describe the magnetization dependence of the charge current.

Averaging (8.46) and (8.47) over the thickness z results in the corresponding electrical resistances, which in the first-order approximation in θ_S^2 are described by the expressions

$$\rho_x = \rho - \frac{\theta_{SH}^2 \tanh A(0)}{A(0)} \left(1 - \frac{\lambda\left(1 - m_y^2\right) \tanh A(0)}{2}\, \mathrm{Re}\, \varphi\left(G_{\uparrow\downarrow}\right)\right) \tag{8.48}$$

$$\rho_y = -\frac{\theta_S^2 \lambda \tanh^2 A(0)}{A(0)} \left(m_x m_y\, \mathrm{Re} - m_z\, \mathrm{Im}\right)\ \varphi\left(G_{\uparrow\downarrow}\right) \tag{8.49}$$

Here, when the N layer thickness increases relatively to the spin-flip diffusion length ($\lambda/d_N \to 0$), $A(0) \to 0$ and SME vanishes. Its magnitude is proportional to the second power of the spin Hall angle and is related to the spin-mixing conductance at the interface.

References

1. Zutic L, Fabian J, Das Sarma S (2004) Spintronics: fundamentals and applications. Rev Mod Phys 76:323
2. Manchon A, Koo HC, Nitta J, Frolov SM, Duine RA (2015) New perspective for Rashba spin-orbit coupling. Nat Mater 36:871
3. Hoffmann A (2013) Spin Hall effects in metals. IEEE 49:5172
4. Tserkovnyak Y, Brataas A, Bauer GE, Halperin BI (2005) Nonlocal magnetization dynamics in ferromagnetic heterostructures. Rev Mod Phys 77:1375
5. Edwards ERJ, Ultrichs H, Demidov VE, Demokritov SO, Urazhdin S (2012) Parametric excitation of magnetization oscillations controlled by pure spin current. Phys Rev B 86:134220
6. Liu L, Pai C-F, Li Y, Ralph DC, Buhram RA (2012) Spin-torque switching with the Giant spin-Hall effect. Science 336:555

7. Liu RH, Lim WL, Urazhdin S (2013) Spectral characteristics of the microwave emission by the spin Hall Nano-oscillator. Phys Rev Lett 110:147601
8. Baither D, Schmitz G, Demokritov SO (2012) Magnetic nanooscillators driven by pure spin current. Nat Mater 11:1028
9. Yang T, Kimura T, Otani Y (2008) Giant spin accumulation signal and pure spin-current-induced reversible magnetization at switching. Nature Phys 4:851
10. Ebrahim-Zaden E, Urazhdin S (2013) Optimization of Pt-based spin-Hall effect spintronic devices. Appl Phys Lett 102:13402
11. Volkov NV (2012) Spintronics: manganite-based magnetic tunnel structures. PHYS-USP 55:250
12. Hirsch JE (1999) Spin Hall effect. Phys Rev Lett 83:1834
13. Chudnovsky EM (2007) Theory of spin Hall effect. Phys Rev Lett 99:206601
14. Miron IM, Gaudin G, Auffer S, Rodmacq B, Schuhl A, Pizzini S, Vogel J, Gambardalla P (2010) Current-driven spin torque induced by the Rashba effect in ferromagnetic metal layer. Nat Mater 9:230
15. Manchon A, Zhang S (2009) Theory of spin torque due to spin-orbit coupling. Phys Rev B 79:094422
16. Wang X, Manchon A (2012) Diffusive spin dynamics in ferromagnetic thin films with a Rashba interaction. Phys Rev Lett 108:117201
17. Cheng R, Zhu J-G, Xiao D (2016) Dynamic feedback in Ferromagnet/spin-Hall Heterostructures. Phys Rev Lett 117:097202
18. Gomonay HV, Loktev VM (2010) Spin transfer and current-induced switching in antiferromagnets. Phys Rev B 81:144427
19. Brataas A, Bauer GEW, Kelly PJ (2006) Non-collinear magnetoelectronics. Phys Rep 427:157
20. Gambardella P, Miron IM (2011) Current-induced spin-orbit torque. Phil Trans R Soc A 369:3175
21. Ou Y, Ralph DC, Buhram RA (2012) Strong spin Hall effect in the antiferromagnetic PtMo. Phys Rev B 93:220405
22. Ando K, Takahashi S, Harii K, Sasage K, Ieda J, Maekawa S, Saitosh E (2008) Electric manipulation of spin relaxation in a film using spin-Hall effect. Phys Rev Lett 101:036601
23. Cheng R, Xiao D, Brataas A (2015) Terahertz Antiferromagnetic Spin Hall Nano-Oscillator. Phys Rev Lett 116:207603
24. Tserkovnyak YA, Bender SA (2014) Spin Hall phenomenology of magnetic dynamics. Phys Rev B 90:014428
25. Tserkovnyak YA, Brataas A, Bauer EW (2002) Spin pumping and magnetic dynamics in metallic multilayers. Phys Rev B 66:224403
26. Cheng R, Xiao D, Niu Q, Brataas A (2014) Spin pumping and spin-transfer torques in Antiferromagnets. Phys Rev Lett 113:057601
27. Mosendz O, Vlaminck V, Pearson JE, Fradin FY, Bauer GEW, Bader SD, Hoffmann A (2010) Detection and quantification of the inverse spin Hall effect from spin pumping in permalloy/normal metal bilayers. Phys Rev B 82:214403
28. Brouver PW (1998) Scattering approach to parametric pumping. Phys Rev B 58:R10135
29. Demidov VE, Urazhdin S, Ulrichs H, Tiberkevich V, Slavin A, Baither D, Schmitz G, Demokritov SO (2012) Magnetic nano-oscillator driven by pure spin current. Nat Mater 11:1028
30. Pai C-F, Liu L, Tseng HW, Ralph DC, Buchram BA (2012) Spin transfer torque devices utilizing the giant spin Hall effect of tungsten. Appl Phys Lett 101:082407
31. Kim K-W, Moon J-H, Lee K-J, Lee H-W (2012) Prediction of Giant spin motive force due to Rashba spin-orbit coupling. Phys Rev Lett 108:21722
32. Wong CH, Tserkovnyak YA (2009) Hydrodynamic theory of coupled current and magnetization dynamics in spin-textured ferromagnets. Phys Rev B 80:184411
33. Wang HL, Due CH, Pu Y, Adur R, Hammel PC, Yang FV (2014) Scaling of spin Hall angle in 3d, 4d and 5d metals from $Y_3Fe_5O_{12}$/metals spin pumping. Phys Rev Lett 112:197201

34. Brataas A, Tserkovnyak YA, Bauer EW, Halperin PC (2014) Spin battery operated by ferromagnetic resonance. Phys Rev B 66:060404
35. Vietstra N, Shan J, Castel V, Wees V-T, Yousset JB (2013) Spin-Hall magnetoresistance in platinum yttrium iron garnet: dependence on platinum thickness and in-plane/out-of-plane magnetization. Phys Rev B 87:184421
36. Nakayama H, Althammer M, Chen Y-T, Uchida K, Kajiwara Y, Kikuchi D, Ohtani T, Geprags S, Opel M, Takahashi S, Gross R, Bauer GEW, Goennenwein STB, Saitosh E (2013) Spin Hall Magnetoresistance induced by a Nonequilibrium proximity effect. Phys Rev Lett 110:206601
37. Chen YT, Takahashi S, Nakayama N, Althammer M, Goennenwein STB, Saitosh E, Bauer GEW (2013) Theory of spin Hall magnetoresistance. Phys Rev B 87:14411
38. Jungfleisch MB, Lauer V, Neb R, Chumak AK, Hillebrands B (2013) Improvement of the yttrium iron garnet/platinum interface for spin-pumping application. Appl Phys Lett 103:022411